Journal of Science and Technology in Civil Engineering, HUCE (NUCE), 2023, 17 (1): 26–40

GRAIN BOUNDARY STRENGTHENING OF MICROSTRUCTURE PHASES IN SS400 STRUCTURAL STEEL WELD ZONE

Nguyen Ngoc Vinh[a,*], Duong Hong Quan[a]

[a]*Faculty of Advanced Technology and Engineering, VNU Vietnam Japan University, Nam Tu Liem, Ha Noi, Viet Nam*

Article history:
Received 14/11/2022, Revised 17/12/2022, Accepted 20/12/2022

Abstract

Grain boundary strengthening is a method of strengthening materials by changing their average crystalize (grain) size, exhibiting the basic relationship between yield stress and the grain size of the materials. This methodology is based on the observation of grain boundaries that are insurmountable borders for dislocations and the number of dislocations located within a grain. Applying this methodology to the structural steel weld zone, the mechanical properties of each microstructural phase can be evaluated through the values of grain diameter. For structural steel weld zones, there are not many methods to directly determine the mechanical properties of microstructural phases. Thus, in this study, a methodology was created to evaluate the values of the yield stress of materials based on the grain boundary strengthening equation. This method was constructed by observing the average grain size and determining the mechanical properties of three microstructural phases in the weld zone (i.e. based metal, heat-affected zone, and weld metal). The results from this study provide an easy way for engineers, architects, and scientists to evaluate the values of mechanical properties of based metal, heat-affected zone, and weld metal in the SS400 structural steel weld zone.

Keywords: cyclic loading; dislocation cell; dislocation density; grain boundary strengthening; microstructure; indentation.

https://doi.org/10.31814/stce.nuce2023-17(1)-03

1. Introduction

Structural steel is applied in many different structural projects such as buildings, bridges, mines, the auto industry, and so on, because of its favorable physical properties, for example, high durability, toughness, and ductility [1–5]. The mechanical properties of structural steel are strongly dependent on both service conditions and metallurgical factors, which include temperature, environmental conditions, and especially the historical loading state [6, 7]. To connect the steel members, welding was attributed to being an efficient method since it is fast and simple in the design. Pham et al. [8] pointed out that the microstructure of the weld zone was complex and included three main microstructural phases such as based metal (BM), Heat-affected zone (HAZ), and weld metal (WM). This can lead to the microstructural inhomogeneous and variation of mechanical properties across the weld joint [3]. Furthermore, the weld joint was also considered to be the weakest link because of its microstructural inhomogeneous and the appearance of local stress concentration in the weld zone, leading to crack

*Corresponding author. *E-mail address:* nn.vinh@vju.ac.vn (Vinh, N. N.)

propagation. As mentioned before, the weld zone is mainly composed of three main microstructural phases, i.e., BM, HAZ, and WM. Among them, the microstructures formed in the WM and HAZ regions play an important role in controlling material properties. These properties consist of elastic modulus (E), yield strength (σ_y), strain hardening exponent (n), and indentation hardness (H). Due to the differences in microstructures in the region of HAZ and WM, mechanical properties of these regions are different when compared to the BM region in the weld zone. For the WM region, typical microstructures mainly include grain boundary ferrite, Widmanstatten ferrite, acicular ferrite, and a small amount of pearlite [9]. The HAZ contains Widmanstatten ferrite, large grains of ferrite, and colonies of pearlite [10–13]. It can be seen that the grain size of HAZ is relatively greater than those in the WM region, and the shape of the Ferrite grains is more uniform. Some researchers pointed out that the mechanical properties of materials depended on both metallurgical factors and operation conditions, including environment, load history, and temperature [6, 14]. During the service life, these conditions can cause the degradation of not only the material properties but also the crack propagation in the structural steel weld zone. Thus, there is a lot of attention on the studies on mechanical properties of microstructural phases as well as the influences of operating factors on the microstructural change in the structural weld zone [5, 7, 15–18].

In the late 1990s, Huang et al. [19] studied the inelastic properties of SS400 structural steel weld joints under cyclic gradient stress. The authors used different strength ranges to simulate the case of a sudden extreme earthquake and the results indicated that although weld connection doesn't influence the loading capacity and inelastic deformation capacity for the plain strength steels, weld connection dramatically reduces the inelastic deformation capacity for high-strength steels. An experimental investigation was carried out to determine the important factors that cause cracking and breakage of SS400 steel members under repeated and large deformation [20]. The experimental data showed that the energy dissipation capacity depended on the entire history of loading, the failure mode, the slenderness ratio, and the width-to-thickness ratio. Pham et al. [17] used the depth-sensing instrumented indentation experiment to estimate the microstructural composition of three microstructural phases in the structural steel weld zone. This research indicated that there is no influence of the size, shape, and grain orientation on the elastic modulus of both ferritic phases; however, these orientations have a significant influence on the stiffness of the ferritic phases [17]. Pham and Kim [21] conducted a series of experiments such as a room temperature low cyclic fatigue (LCF), indentation, tensile testing, optical microscopy examination, and finite element methodology (FEM) to investigate the microstructure and mechanical properties in SS400 structural weld zone under low-cycle fatigue. The results from Pham and Kim's study showed that mechanical properties of the WM region were higher than those in the BM region, while the other properties of HAZ decreased from the WM region to the BM region [21]. Recently, Nguyen et al. [5] employed the definition of strain rate sensitivity to investigate the influences of loading rate on mechanical properties of BM, HAZ, and WM subjected to fatigue conditions. Strain rate sensitivity is defined as the change in the mechanical properties to the change of strain rate ($\dot{\varepsilon}_I$) at a given temperature and is described as $m = dH/d\dot{\varepsilon}_I$. The experimental results showed that when the strain amplitude increased from 0.4% to 1.0%, strain rate sensitivity tended to decrease from 0.042 to 0.028, respectively. Moreover, the micromechanism was also proposed to further explain the variation of mechanical properties under different fatigue conditions by showing the relationship between the strain rate sensitivity and dislocation cell size (d') as $m = \dfrac{3\sqrt{3}K_bT}{\alpha\mu bcKV^*}d'$, where K_b and T are Boltzmann's constant and the absolute temperature; V^* is an activation volume; c is Tabor's factor; α, μ, b, and K are material constant.

However, there are not many methodologies to determine directly the mechanical properties of microstructural phases due to the small size of the structural steel weld zone. Furthermore, advanced instrumented machines, such as depth sensing nanoindentation, are not available, leading to the difficulty in the determination of mechanical properties of BM, HAZ, and WM regions. Since the limitation of mechanical properties of the weld zone, the engineers, architects, and designers ignored these properties of the weld zone in the hall structures. Therefore, it is necessary to have a comprehensive study to propose a methodology that allows determining the mechanical properties of microstructural phases based on the information of grain size and to characterize the variation of dislocation lines subjected to the cyclic loading for three main microstructural components.

2. Methodology

Nanoindentation technology is recently used to determine the mechanical properties of the materials based on the indentation responses, i.e., apply load-penetration depth curves as seen in Fig. 1 [4, 22–26]. Generally, Kick's law, $P = Ch^k$, is used to describe the loading part, while $P_u = B(h - h_r)^m$ is also employed to describe the unloading curve [22, 27–33], where C is the load curvature; h is the penetration depth of the indentation; P is the applied load, and k is the exponential factor ranging from 1.5 to 2; h_r is the final depth; B and m are constant coefficients. Based on the indentation responses, hardness and elastic modulus of the materials can be calculated using Eq. (1) and Eq. (2), respectively. For plastic properties of materials, the inverse algorithm and dimensionless function can be used to evaluate the values of yield stress σ_y, and strain hardening exponent n as illustrated in Eqs. (3) and (4) [17, 34].

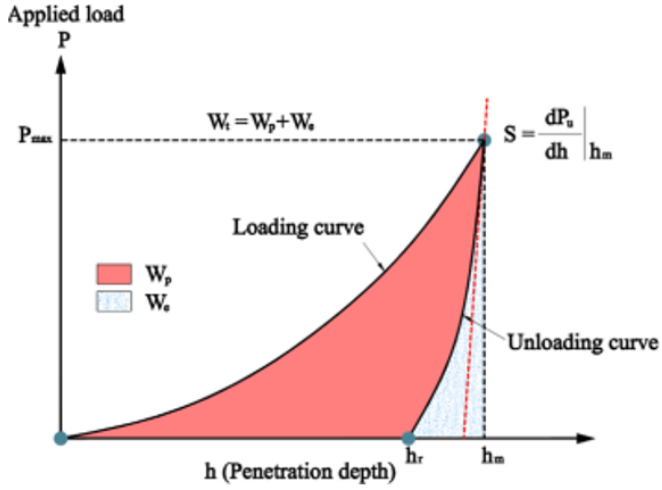

Figure 1. A typical load-displacement curve (P-h) of structural steel from nanoindentation experiment

$$H = \frac{P_m}{A_c} \tag{1}$$

$$E = \left(1 - \vartheta^2\right)\left[\frac{1}{E_r} - \frac{1 - \vartheta_i^2}{E_i}\right]^{-1} \tag{2}$$

$$\frac{E_r^*}{\sigma_y} = \Pi_1 = \sum_{i=1}^{4}\sum_{j=1}^{4}\sum_{k=1}^{3}\left[a_{ijk}n^{j-1}\alpha^{k-1}\left(\frac{E_r}{C}\right)^{i-1}\right] \tag{3}$$

$$\frac{S}{E_r^* h_m} = \Pi_2 = \sum_{i=1}^{4}\sum_{j=1}^{4}\sum_{k=1}^{3}\left[b_{ijk}n^{j-1}\alpha^{k-1}ln\left(\frac{E_r}{\sigma_y}\right)^{i-1}\right] \tag{4}$$

In Eqs. (1)–(4), h_c is contact depth; A_c is contact area; P_m is maximum applied load; ϑ and ϑ_i are Poisson's ratio of the indented material and indenter; E_i is the elastic modulus of the indenter; E_r is reduced modulus; S is the initial unloading slope described as $S = dP_u/dh|_{h_m}$; β is a correction factor for indenter shape; a_{ijk} and b_{ijk} are the coefficients; α is defined as the strain at the start of the stiff strain ε_{st} divided by the initial yield strain ε_y [17].

In this study, a methodology is proposed to determine the values of material properties in the weld zone based on the values of microstructural grain size d. Normally, the variation of microstructure can be observed by using the optical microscope examination. Based on the micro images from optical microscope examination, microstructural grain size of BM and HAZ can be determined using the straight-line method [35]. Since WM includes polymorphic ferrite (α), Widmanstatten ferrite (α_w), and lenticular ferrite (α_a) with different shapes and sizes [36], it is difficult to determine the grain size in this region. Therefore, the straight-line method does not seem to be appropriate to determine the grain size in the WM region. Fortunately, the appearance of the circle method [35] can overcome this challenge. As a result, the circle method was used to determine the average grain size in the WM region in this study. It should be noted that at least 3 circles can be used for each microimage to estimate the average diameter of the grain. The formula of this circle method can be described as $d = (C \times \pi)/(2 \times N \times M)$, where C is the diameter of the circle, N is the number of lines that intersect the circle, M is the scale of the microstructure [35]. The dislocation density (ρ) and dislocation cell size (d) can be calculated based on the micrographs and their sketches of the dislocation structure. Nguyen et al. [5] point out that dislocation density can be calculated using the following equation

$$\rho = \frac{N_{Intersection}}{A} \tag{5}$$

where A and $N_{Intersection}$ are a checked area and the intersection number of the dislocation lines to the surface plane, respectively. It should be noted that both values of $N_{Intersection}$ and A are directly obtained from micro-images.

3. Results and Discussion

3.1. Relationship between grain size and mechanical properties of the weld zone

Fig. 2 shows optical microscopy images of the microstructure of BM, containing ferrite grains and small regions of pearlite (α-ferrite + Fe_3C cement), in which a small amount of pearlite is located at the grain boundary edges or the corners of the ferrite grain [36]. Based on the microimages in Fig. 2, the average grain diameter of the BM region was well calculated using the straight-line method [35]. As a result, d = 12.83 μm ± 2.18 μm was reported for the BM region. Similarly, the HAZ region composes of polygonal ferrite (PF) grains with different degrees of reflected color brightness as seen in Fig. 3. It can be recognized that ferrite grains in the HAZ region are relatively smaller than those observed in the BM region. Furthermore, there are two types of phase changes that occur in the HAZ during the cooling process. The first one is the high-temperature conversion from $\delta - Fe$ to $\gamma - Fe$, and the second phase is the conversion from $\gamma - Fe$ to $\alpha - Fe$ [36]. The averaged grain size of the HAZ region was determined from the microimages using the straight-line method to be 9.3 μm ± 1.5 μm.

The microstructure of WM is completely different from other phases as observed in Fig. 4. It can be seen that WM mainly contains ferrite grains with different sizes and shapes and a certain small amount of pearlites. These Ferrite grains were divided into several types, for example, polymorphic ferrite (α), Widmanstatten ferrite (α_w), and lenticular ferrite (α_a) [36]. By using the circle method, the mean grain size of the WM region was well reported to be 2.99 μm ± 0.61 μm. It can be recognized from the variation of grain size crossing the weld joint that the mean grain size tends to decrease from the BM region to the WM region, while the value of the HAZ region gradually decreases from the BM region to the WM region. Another interesting feature of the microstructural evolution in the weld joint is that the variation of grain size in the region from HAZ to WM seems to be greater than that in the region from BM to HAZ.

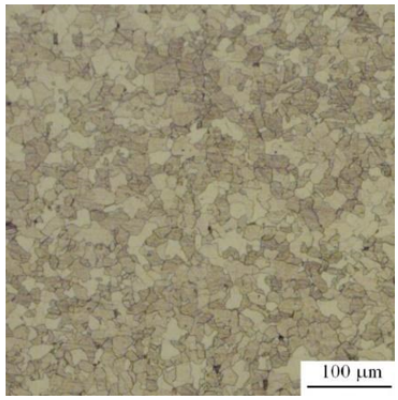

Figure 2. Optical microscopy images of microstructures of BM

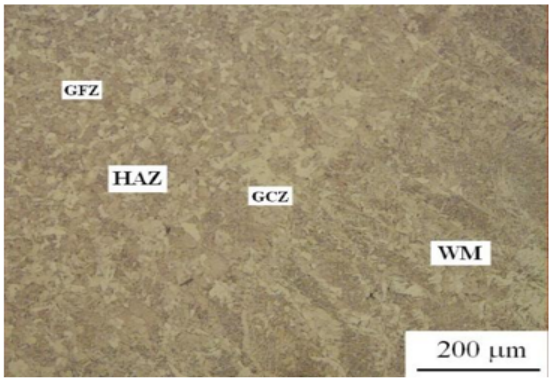

(a) Scale bar of 200 μm

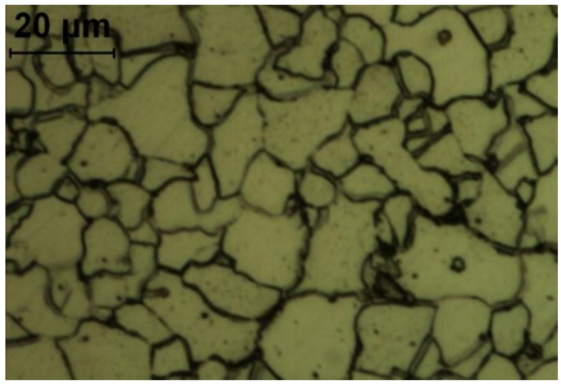

(b) Scale bar of 20 μm

Figure 3. Optical microscopy images of microstructures of HAZ

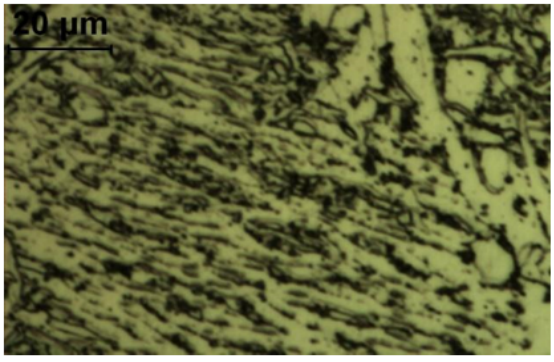

(a) Scale bar of 200 μm

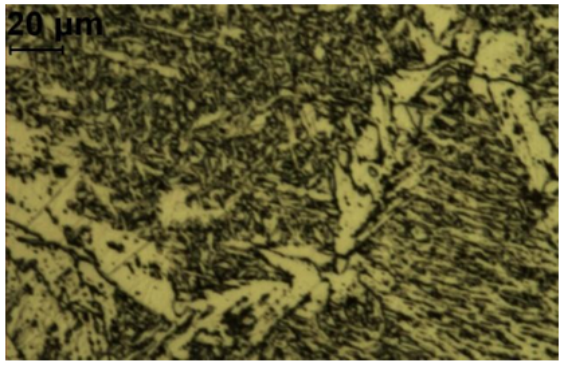

(b) Scale bar of 20 μm

Figure 4. Optical microscopy images of microstructures of WM

Table 1. Average data mechanical properties in the weld zone

Mechanical Properties	BM	HAZ	WM
E (GPa)	207.5	212.2	218.3
H (GPa)	2.0	2.2	2.7
σ_y (MPa)	302.6	331.2	403.4
n	0.191	0.196	0.204

To construct the grain boundary strengthening equation of the SS400 structural steel weld zone, the information on grain size and mechanical properties of each microstructural phase is necessary to build the relationship between the grain size and yield stress. For this purpose, depth-sensing instrumented experiments were conducted on three main regions in the weld zone, for example, BM, HAZ, and WM. Based on the indentation response, the mechanical properties of these microstructural phases were determined using Eqs. (1)–(4). As a result, the values of yield stress, hardness, elastic modulus, and work hardening were obtained as listed in Table 1. It can be seen that both H and σ_y of

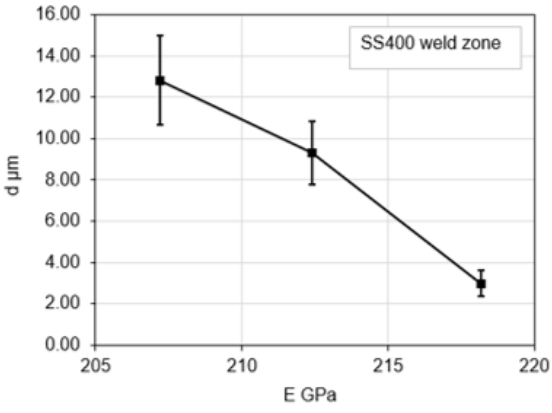

(a) Relationship between d and E

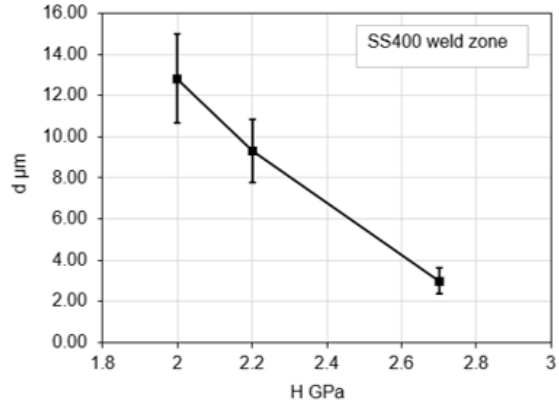

(b) Relationship between d and H

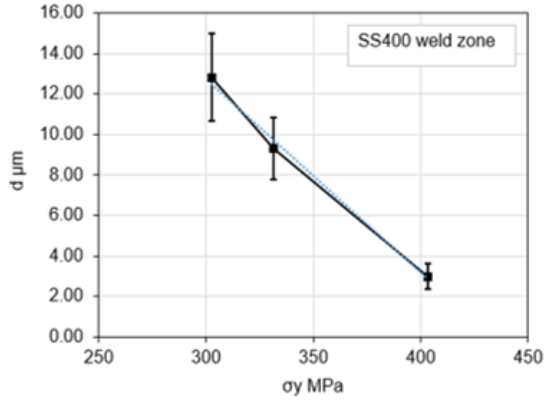

(c) Relationship between d and σ_y

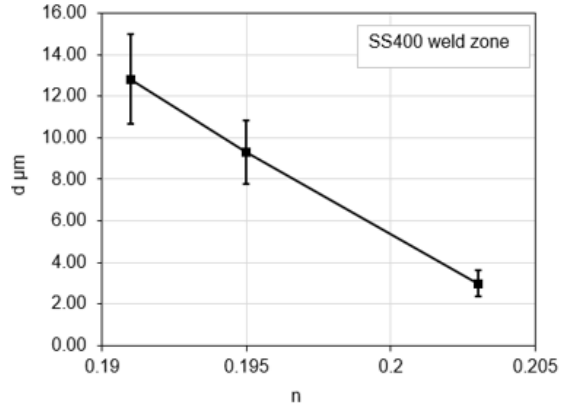

(d) Relationship between d and n

Figure 5. Relationship between the grain diameter and the mechanical properties

BM are the smallest, while the WM region has the highest values compared to other microstructural phases in the weld joint. This trend is in good agreement with the results reported in the literature [10, 37]. Combined with the variation of grain size in the weld zone, the relationship between mechanical properties and grain size was well constructed as shown in Fig. 5.

It can be observed that E decreases from 218.2 GPa to 207.2 GPa when the grain size increases from 2.99 μm ± 0.61 μm to 12.83μm ± 2.18 μm. It means that E is inverse-proportional to the grain size. Furthermore, the relationship between E and grain size seems to be nonlinear as seen in Fig. 5(a). A similar observation for the relationship between σ_y, H, n, and grain size can be seen in Figs. 5(b), 5(c), and 5(d), respectively. When the grain size increases in the range of 2.99–12.83 μm, H decreases from 2.7 GPa to 2 GPa, while σ_y decreases from 403.4 MPa to 302.6 MPa. Additionally, n tends to increase from 0.191 to 0.204 with the decrease of grain size from 12.83 μm ± 2.18 μm to 2.99 μm ± 0.61 μm. It can be deduced that mechanical properties of microstructural phases tend to increase when the grain size becomes smaller.

3.2. Grain boundary strengthening equation in the weld zone

Grain boundary strengthening (or Hall–Petch strengthening) is generally employed as a methodology to strengthen materials through a change in their mean grain (crystallite) size, in which the change of grain size can influence the number of dislocations piled up at the grain boundary and yield stress [38]. Thus, the yield stress-grain size relationship can be mathematically described by the Hall–Petch equation as follows [38, 39]:

$$\sigma_y = \sigma_0 + \frac{k_y}{\sqrt{d}} \tag{6}$$

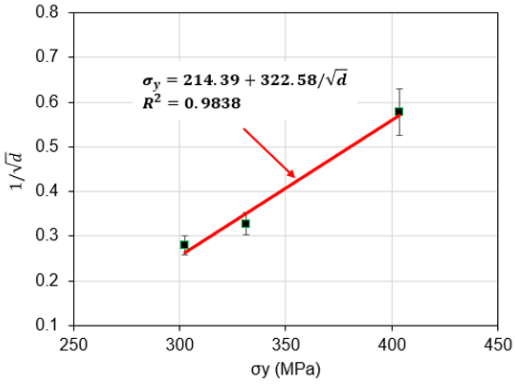

Figure 6. Plot of $1/\sqrt{d}$ versus yield stress to determine the Hall–Petch equation using regression analysis

In Eq. (6), σ_0 is a material constant for the starting stress for dislocation movement and k_y is the strengthening coefficient [38]. Since the main purpose of this study is to find out the relationship between mechanical properties and grain size, the regression analysis was employed to evaluate the parameters of Eq. (6), and the results were shown in Fig. 6. It should be noted that the correlation between σ_y and $1/\sqrt{d}$ was employed to reduce the complexity of the regression analysis. Thus, the linear relation of yield stress and $1/\sqrt{d}$ was employed instead of the original relation of grain boundary strengthening relation. As seen, the relationship between σ_y and $1/\sqrt{d}$ can be well described by using the following equation

$$y = 0.0031x - 0.6646 \tag{7}$$

As a result, the strengthening equation for weld joint was logically described as

$$\sigma_y = 214.39 + 322.58/\sqrt{d} \tag{8}$$

Eq. (8) describes well the experimental data in the weld zone with a standard deviation of 0.984. Furthermore, the values of material constant σ_0 and the strengthening coefficient k_y were determined via the regression analysis results as 214.39 and 322.58, respectively. Thus, Eq. (8) was recommended

to describe the grain boundary strengthening relationships in the SS400 structural steel weld zone. It can be observed from the variation of mean grain size (Figs. 2–5) and the variation of mechanical properties in the weld zone that yield stress tended to increase from the BM (302.6 MPa) to the WM (403.4 MPa), while means grain size showed a decrease from 12.83 μm ± 2.18 μm to 2.99 μm ± 0.61 μm, respectively. It means that the yield stress and mean grain size are inversely proportional to each other.

To confirm the accuracy of the present study, the strengthening equation for SS400 structural steel weld zone was compared to the results reported in the literature [36, 40]. The results indicated that the strengthening equation described well the correlation between yield stress and grain size with a maximum relative error of 3.82%. The maximum relative error being less than 5% ensures the high accuracy of the grain boundary strengthening equation of the SS400 structural steel weld zone in this study. Therefore, this equation can be used to predict the values of mechanical properties of microstructural phases based on the values of grain size, which can be easily obtained from the micro images of microstructure.

Table 2. Validation of present grain boundary strengthening equation

	d (μm)	σ_y (MPa)	Prediction of present study (MPa)	Relative error (%)
Pham et al. [36]	17.5	302.70	291.50	3.70
Nguyen et al. [40]	18	301.95	290.42	3.82

3.3. Variation of mechanical properties of SS400 structural steel weld zone under low-cycle fatigue

In this section, the variation of mechanical properties of SS400 structural steel weld zone was investigated by performing the nanoindentation experiments on the fatigue specimens at the strain amplitude of 0.4%, 0.6%, 0.8%, and 1.0%. It should be noted that all nanoindentation experiments were performed at the same loading rate of 0.04/s and these tests must be conducted as soon as finishing the polishing process to reduce the influence of oxidation. The results of indentation experiments were presented in Fig. 7. As seen, when the strain amplitude increases from 0.4% to 1%, the larger applied load and indentation depth can be observed. Indeed, at the strain amplitude of 0.4%, the maximum applied load can be observed to be 183.239 mN, and the maximum indentation depth can be obtained to be 2057.55 nm. Furthermore, at the strain amplitude of 0.6%, the maximum applied load

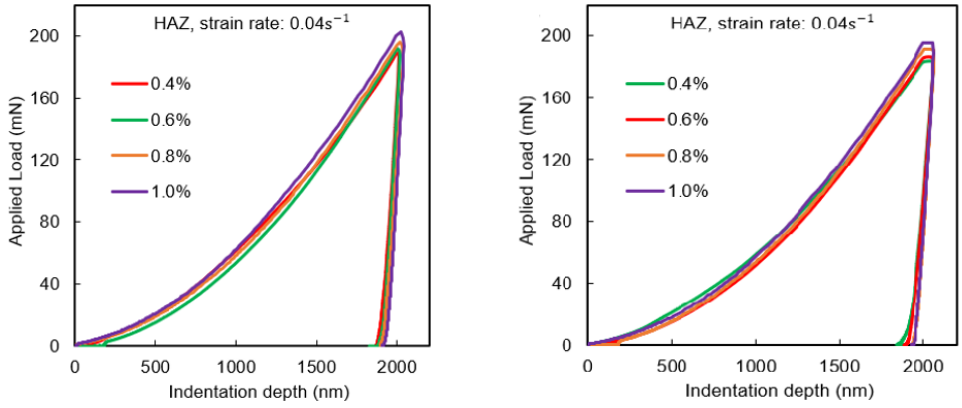

(a) Series #1 (b) Series #2

Figure 7. Indentation curves of microstructural phases in SS400 structural steel weld zone

is 186.133 mN, while the largest penetration depth can be obtained being 2054.65 nm. When the strain amplitude increase to 0.8%, the maximum applied load can maximum displacement can be recorded as 191.701 mN and 2047.36 nm, respectively. At the highest strain amplitude, the maximum applied load reaches 195.527 mN, corresponding to the maximum indentation depth of 2056.28 nm. From the experimental data, it can be inferred that the applied load and indentation depth both tend to increase with the increase of strain amplitude. The same behavior can be observed for series #2 of indentation curves presented in Fig. 7(b). Based on these indentation responses, mechanical properties of material can be determined using Eqs. (1)–(4), resulting in the relationship between mechanical properties and fatigue condition was well constructed in Figs. 8 and 9.

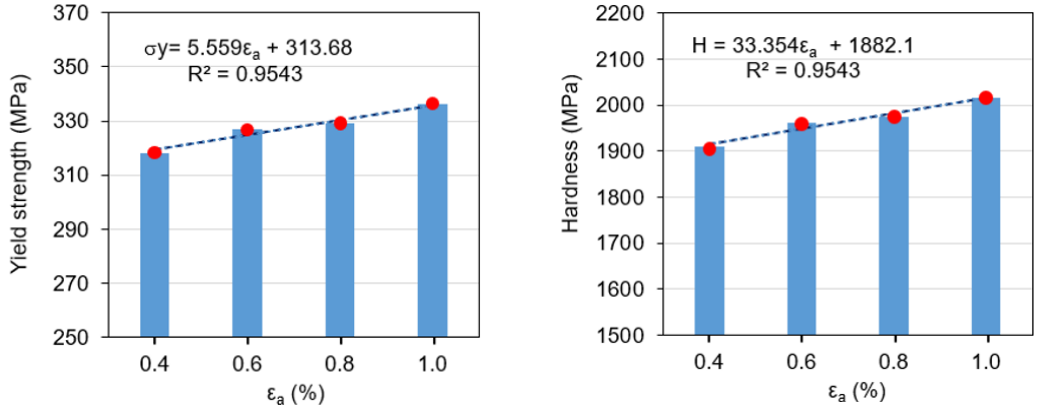

(a) Variation of yield strength

(b) Variation of hardness

Figure 8. The influences of cyclic loading on mechanical properties for series #1

It can be observed from Fig. 8(a) that σ_y tends to increase from 318.30 MPa to 336.15 MPa when the strain amplitude gradually increases from 0.4% to 1.0%. The variation of yield stress seems to be linear as illustrated in Fig. 8(a) and described in Eq. (10). Similarly, the same behavior of hardness can be observed in Fig. 8(b). Indeed, when the strain amplitude increases from 0.4% to 1.0%, H increases from 1909.80 MPa to 2016.91 MPa, respectively. The linear increase of hardness with the increase of strain amplitude can be described using the linear equation, Eq. (10), and the equation parameters can be obtained using the regression analysis. In Eqs. (9) and (10), ε_a is the strain amplitude of the low-cycle fatigue testing. It can be seen that Eq. (9) describes well the experimental data of yield stress of three main microstructural phases in the SS400 structural steel weld zone. Similarly, the observation for hardness can be found in Fig. 8(b).

$$\sigma_y = 5.559\varepsilon_a + 313.68 \tag{9}$$

$$H = 33.354\varepsilon_a + 1882.1 \tag{10}$$

From the data obtained in Fig. 7(b), Eqs. (1)–6 calculate the mechanical properties of the material under cyclic loading, and the results were shown in Fig. 9. It can be observed that the yield strength σ_y value also tends to increase from 342.37 MPa to 362.40 MPa when the strain amplitude gradually increases from 0.4% to 1.0%. This growth trend can also be seen in Fig. 9(b), indeed when the strain amplitude increases gradually from 0.4% to 1.0%, the trend of hardness H increases from 2054.20 MPa to 2174.42 MPa. The variation of yield stress and hardness under strain amplitude can

be described using the equations as follows

$$\sigma_y = 6.3645\varepsilon_a + 336 \tag{11}$$

$$H = 38.187\varepsilon_a + 2016 \tag{12}$$

Eqs. (11) and (12) describe well the experimental data in the weld zone with a standard deviation of 0.9742.

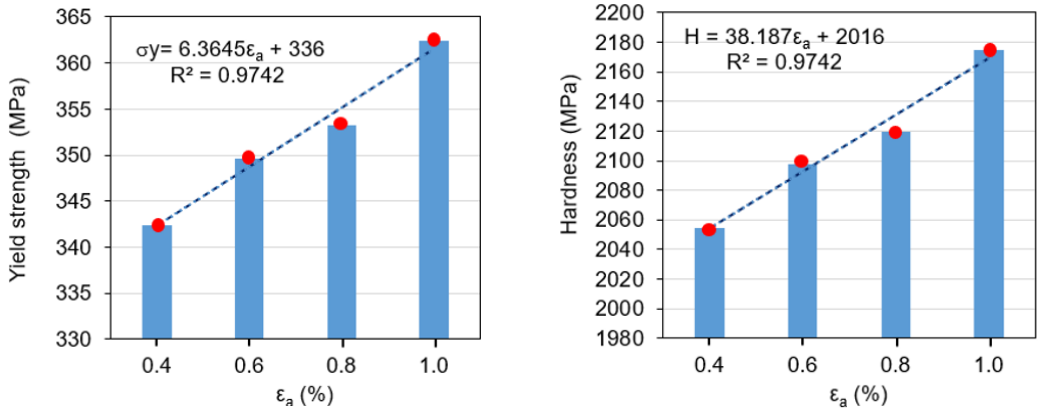

(a) Variation of yield strengt

(b) Variation of hardness

Figure 9. Influences of cyclic loading on mechanical properties for series #2

3.4. Microstructure evolution of SS400 weld zone under cyclic loading

The basic correlation between the damaged microstructure and the degradation of mechanical properties of the SS400 structural steel weld zone strongly depends on the strain amplitude of cyclic loading. Therefore, the dislocation structure of the damaged samples at different strain amplitude levels was observed and investigated by using optical microscopy examination. The results of optical microscope examination were illustrated as seen in Fig. 10.

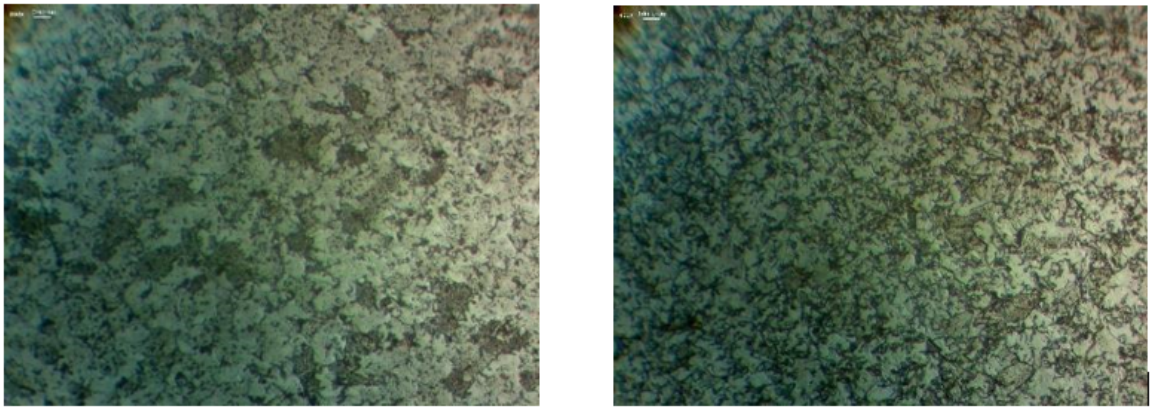

(a) Microstructure of BM region at a strain amplitude of 0.4%

(b) Microstructure of BM region at a strain amplitude of 1%

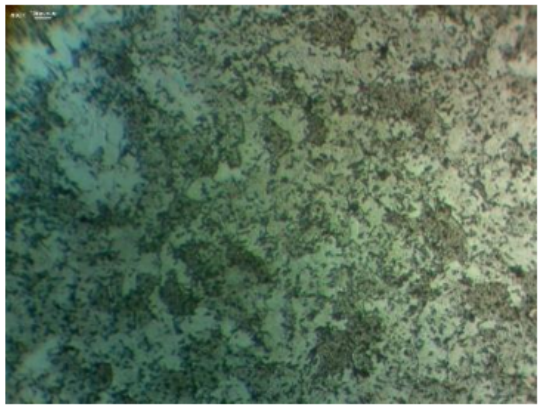

(c) Microstructure of HAZ region at a strain amplitude of 0.4%

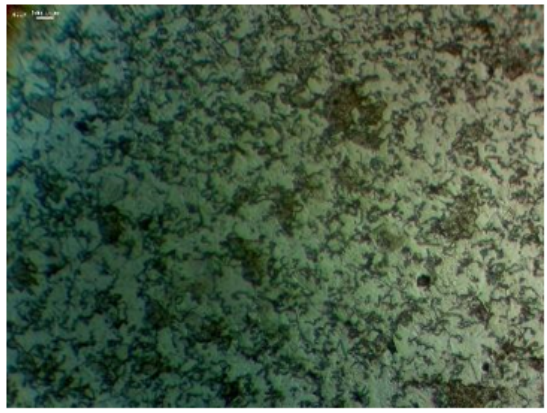

(d) Microstructure of HAZ region at a strain amplitude of 1%

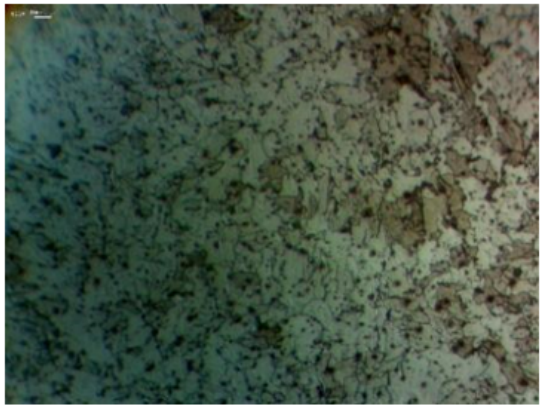

(e) Microstructure of WM region at a strain amplitude of 0.4%

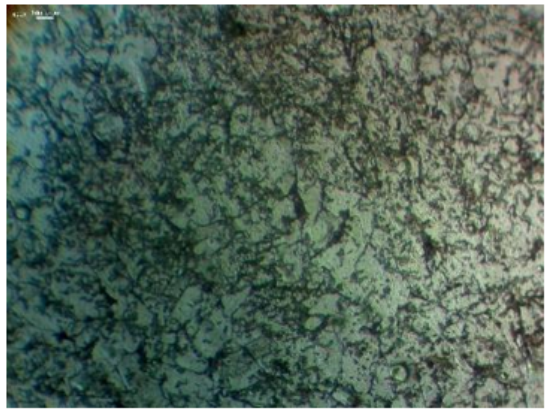

(f) Microstructure of the WM region at a strain amplitude of 1%

Figure 10. Dislocation structure of microstructural phases under cyclic loading

At a strain amplitude of 0.4%, as mentioned before, the grain size of the BM region is larger and the grain size of the WM region is smaller, while the grain size of the HAZ region gradually decreases from the BM region to the WM region. The dislocation density gradually increases from BM to WM as observed in Figs. 10(a), 10(c), and 10(e), respectively. The dislocation lines were developed with a random arrangement. Dislocation lines were detected in the sub-grains resulting in the formation of smaller grain size structures as demonstrated in Figs. 10(a), 10(c), and 10(e). When the strain amplitude increased from 0.4% to 1%, the dislocation structures of BM, HAZ, and WM regions were fully developed as seen in Figs. 10(b), 10(d), and 10(f). It can be seen that the density of dislocation lines at 1% strain amplitude was higher than those at a lower strain amplitude level (0.4%). Furthermore, the sub-grain size was also observed to decrease. It means that the density of dislocation tends to increase as illustrated in Figs. 10(b), 10(d), and 10(f).

Indeed, the dislocation density of the damaged samples was calculated at different strain amplitudes levels, as shown in Fig. 11. It should be noted that the circle method was used to determine the dislocation density of the samples, and further details of this method can be found elsewhere

[35, 41]. The value of dislocation density was obtained from nine different locations with the same diameter. Consequently, the mean values of dislocation density in BM, HAZ, and WM regions at different strain amplitudes (0.4%–1%) were calculated based on these values of the circle method. The analysis results indicated that the mean dislocation density at 0.4% strain amplitude of BM is 37.331 ± 1.397 lines/μm^2. Similarly, the mean dislocation density at 1% strain amplitude of BM is 48.981± 1.226 lines/μm^2. It can be deduced that the dislocation density tended to increase when the strain amplitude increased in the range of 0.4%–1%. The experimental results confirmed the observation of dislocation structure in Fig. 10.

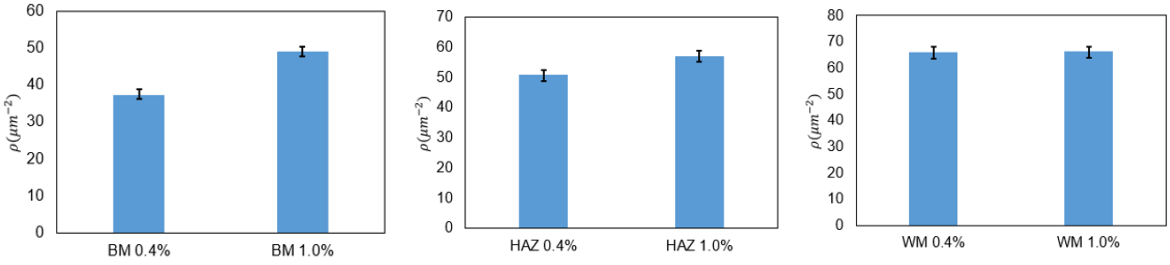

(a) Dislocation density of BM from 0.4% and 1.0%

(b) Dislocation density of HAZ from 0.4% and 1.0%

(c) Dislocation density of WM from 0.4% and 1.0%

Figure 11. Influences of fatigue conditions on dislocation density of BM, HAZ, and WM

Similarly, the microstructure of the HAZ region is at a strain amplitude of 0.4%, and the mean dislocation density of this region is 50.93 ± 1.602 lines/μm^2. When the microstructure of the HAZ region is at a strain amplitude 0.4%, the mean dislocation density of this region is 57.166 ± 2.046 lines/μm^2. The microstructure of the WM region at a strain amplitude of 0.4% , the mean dislocation density of this region is 66.131 ± 2.034 lines/μm^2. The microstructure of the WM region at a strain amplitude of 1%, the mean dislocation density of the region is 66.26 ± 2.244 lines/μm^2. At the same strain amplitude of 0.4%, the mean dislocation density of WM is larger than those in the BM region as observed in Fig. 12(b). Similarly, the mean dislocation density increases from the BM region to the WM region at the same strain applitude of 1% as seen in Fig. 12(a).

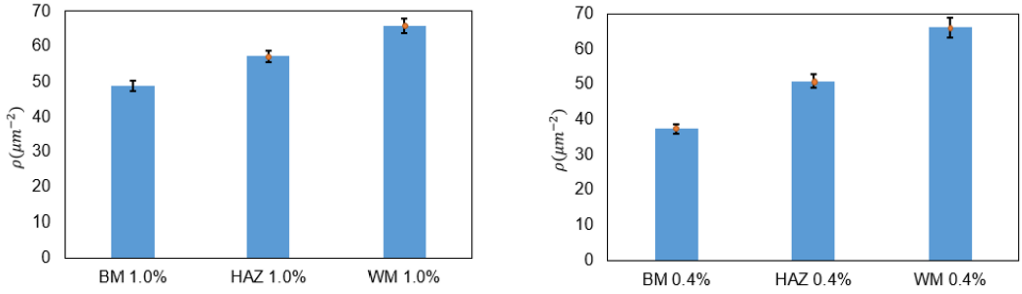

(a) Variation of dislocation density at ε_a = 1%

(b) Variation of dislocation density at ε_a = 0.4%

Figure 12. Dislocation density change of microstructural phases at the same fatigue condition

The relationship between yield stress and dislocation density has been presented through the formula of strain gradient plastic [42]. The formula is built on the dislocation-based Taylor's flow stress

[43], as follows:

$$\sigma = \alpha\mu b\sqrt{\rho_{SSD} + \rho_{GND}} \tag{13}$$

where α is a constant usually assumed to be 0.5 [44]; μ is the shear modulus; b is the magnitude of the Burgers vector; ρ_{SSD} is density Statistically Stored Deviation; ρ_{GND} is density Geometrically Necessary Displacement. In a crystal unit, the GND density is directly related to the plastic strain gradient [45–47]. It can be seen that the yield stress is proportional to the summation of dislocation density since $\alpha\mu b$ is positive for a given material. Indeed, when the strain amplitude increases from 0.4% to 1.0%, the mechanical properties of fatigue specimens increase [48], while the dislocation density tends to increase from 37.331 ± 1.397 lines/μm^2 to 48.981± 1.226 lines/μm^2. It means that the mechanical properties strengthen with the further increase of fatigue condition and yield stress and dislocation density are proportional to each other. This argument confirms the relationship between yield stress and dislocation density as described in Eq. (13).

4. Conclusions

This study provides a simple methodology to estimate the mechanical properties of microstructural phases by constructing the relationship between the yield stress and grain size (strengthening equation). The strengthening equation for SS400 structural steel weld zone was proposed as $\sigma_y = 214.39 + 322.58/\sqrt{d}$. This simple methodology was validated by comparing the yield stress values of SS400 weld zones in the literature. The variation of mechanical properties of SS400 structural steel with the fatigue condition was investigated and discussed. The strain amplitude influences not only the shape but also the magnitude of the loading/unloading curves. When the strain amplitude increased from 0.4% to 1.0%, loading curvature, yield stress, and hardness showed a linear increase while the dislocation density tends to increase from 37.331 ± 1.397 lines/μm^2 to 48.981± 1.226 lines/μm^2.

Acknowledgments

This research has been done under the research project QG.22.25 “Experimental study on the dynamic behavior of microstructural phases in the weld zone under low-cycle fatigue using nanoindentation technology” of Vietnam Nation University, Hanoi.

References

[1] Pham, T.-H., Kim, S.-E. (2015). Nanoindentation for investigation of microstructural compositions in SM490 steel weld zone. *Journal of Constructional Steel Research*, 110:40–47.

[2] Luecke, W. E., McColskey, J. D., McCowan, C. N., Banovic, S. W., Fields, R. J., Foecke, T., Siewert, T. A., Gayle, F. W. (2005). Mechanical properties of structural steel. Technical report.

[3] Pham, T.-H., Kim, S.-E. (2015). Determination of mechanical properties in SM490 steel weld zone using nanoindentation and FE analysis. *Journal of Constructional Steel Research*, 114:314–324.

[4] Nguyen, N.-V., Pham, T.-H. (2020). Experimental study on dynamic nanoindentation on structural weld zone. *IOP Conference Series: Materials Science and Engineering*, 869(3):032027.

[5] Nguyen, N.-V., Pham, T.-H., Kim, S.-E. (2019). Strain rate sensitivity behavior of a structural steel during low-cycle fatigue investigated using indentation. *Materials Science and Engineering: A*, 744:490–499.

[6] Soboyejo, W. (2002). *Mechanical Properties of Engineered Materials*. CRC Press.

[7] Ye, D., Xu, Y., Xiao, L., Cha, H. (2010). Effects of low-cycle fatigue on static mechanical properties, microstructures and fracture behavior of 304 stainless steel. *Materials Science and Engineering: A*, 527 (16-17):4092–4102.

[8] Pham, T.-H., Kim, S.-E. (2017). Characteristics of microstructural phases relevant to the mechanical properties in structural steel weld zone studied by using indentation. *Construction and Building Materials*, 155:176–186.

[9] Nguyen, N.-V., Pham, T.-H., Kim, S.-E. (2019). Microstructure and strain rate sensitivity behavior of SM490 structural steel weld zone investigated using indentation. *Construction and Building Materials*, 206:410–418.

[10] Easterling, K. (1992). *Introduction to the physical metallurgy of welding*. Second edition, Butterworth-Heinemann.

[11] Díaz, M., Madariaga, I., Rodriguez-Ibabe, J. M., Gutierrez, I. (1998). Improvement of mechanical properties in structural steels by development of acicular ferrite microstructures. *Journal of Constructional Steel Research*, 46(1-3):413–414.

[12] Lee, C.-H., Shin, H.-S., Park, K.-T. (2012). Evaluation of high strength TMCP steel weld for use in cold regions. *Journal of Constructional Steel Research*, 74:134–139.

[13] Güral, A., Bostan, B., Özdemir, A. T. (2007). Heat treatment in two phase region and its effect on microstructure and mechanical strength after welding of a low carbon steel. *Materials & Design*, 28(3): 897–903.

[14] Boyer, H. E. (1987). *Atlas of Stress-Strain Curves*. ASM Int. Met. Park. Ohio.

[15] Srinivasan, V., Sandhya, R., Bhanusankararao, K., Mannan, S., Raghavan, K. (1991). Effects of temperature on the low cycle fatigue behaviour of nitrogen alloyed type 316L stainless steel. *International Journal of Fatigue*, 13(6):471–478.

[16] Ye, D., Matsuoka, S., Nagashima, N., Suzuki, N. (2005). Multi-scale deformation behavior investigation of 18Cr–8Ni austenitic steel subjected to low-cycle fatigue loading. *Materials Characterization*, 55(2): 106–117.

[17] Pham, T.-H., Kim, J. J., Kim, S.-E. (2015). Estimating constitutive equation of structural steel using indentation. *International Journal of Mechanical Sciences*, 90:151–161.

[18] Fukumoto, K., Onitsuka, T., Itoh, T., Sakasegawa, H., Tanigawa, H. (2018). Microstructure of fatigue-tested F82H steel under multi-axial loadings. *Nuclear Materials and Energy*, 15:180–184.

[19] Huang, Y. H., Onishi, Y., Hayashi, K. (1996). Inelastic behaviour of HSS with weld connections under cyclic gradient stress. In *11 Th World Conf. Earthq. Eng.*

[20] Park, Y.-S., Park, S.-J., Iwai, S., Kang, S.-H. (2004). Failure and damage of steel thin-plate elements and angle members due to very-low-cycle loading. *Engineering Structures*, 26(11):1623–1632.

[21] Pham, T.-H., Kim, S.-E. (2016). Microstructure evolution and mechanical properties changes in the weld zone of a structural steel during low-cycle fatigue studied using instrumented indentation testing. *International Journal of Mechanical Sciences*, 114:141–156.

[22] Oliver, W. C., Pharr, G. M. (1992). An improved technique for determining hardness and elastic modulus using load and displacement sensing indentation experiments. *Journal of Materials Research*, 7(6):1564–1583.

[23] Nguyen, N.-V., Kim, J. J., Kim, S.-E. (2019). Methodology to extract constitutive equation at a strain rate level from indentation curves. *International Journal of Mechanical Sciences*, 152:363–377.

[24] Nguyen, N.-V., Pham, T.-H., Kim, S.-E. (2019). Microstructure and strain rate sensitivity behavior of SM490 structural steel weld zone investigated using indentation. *Construction and Building Materials*, 206:410–418.

[25] Vinh, N. N., Anh, V. Q., Thang, H. T. (2020). Characterization of strain amplitude-dependent behavior of hardness and indentation size effect of SS400 structural steel. *Journal of Science and Technology in Civil Engineering (STCE) - HUCE*, 14(3):15–25.

[26] Hoan, P. T., Vinh, N. N., Tung, N. T. T. (2019). Indentation for investigation of strain rate effect on mechanical properties in structural steel weld zone. *Journal of Science and Technology in Civil Engineering (STCE) - HUCE*, 13(3):104–112.

[27] Lee, J., Lee, C., Kim, B. (2009). Reverse analysis of nano-indentation using different representative strains and residual indentation profiles. *Materials & Design*, 30(9):3395–3404.
[28] de la Incera, V., Alarcon, R., Cole, P. L., Djalali, C., Umeres, F. (2007). Magnetic Phases in Dense Quark Matter. In *AIP Conference Proceedings*, AIP.
[29] Cheng, Y.-T., Cheng, C.-M. (2004). Scaling, dimensional analysis, and indentation measurements. *Materials Science and Engineering: R: Reports*, 44(4-5):91–149.
[30] Ogasawara, N., Chiba, N., Chen, X. (2006). Measuring the plastic properties of bulk materials by single indentation test. *Scripta Materialia*, 54(1):65–70.
[31] Antunes, J., Fernandes, J., Menezes, L., Chaparro, B. (2007). A new approach for reverse analyses in depth-sensing indentation using numerical simulation. *Acta Materialia*, 55(1):69–81.
[32] Bucaille, J. L., Stauss, S., Felder, E., Michler, J. (2003). Determination of plastic properties of metals by instrumented indentation using different sharp indenters. *Acta Materialia*, 51(6):1663–1678.
[33] Hosseinzadeh, A. R., Mahmoudi, A. H. (2017). Determination of mechanical properties using sharp macro-indentation method and genetic algorithm. *Mechanics of Materials*, 114:57–68.
[34] Truesdell, C. C. *The Pi Theorem of Dimensional Ana sis*. (n.d.).
[35] ASTM E112 (2010). *Standard Test Methods for Determining Average Grain Size E112-10*. ASTM E112-10. 96.
[36] Pham, T.-H., Kim, J. J., Kim, S.-E. (2014). Estimation of microstructural compositions in the weld zone of structural steel using nanoindentation. *Journal of Constructional Steel Research*, 99:121–128.
[37] Kim, J. J., Pham, T.-H., Kim, S.-E. (2015). Instrumented indentation testing and FE analysis for investigation of mechanical properties in structural steel weld zone. *International Journal of Mechanical Sciences*, 103:265–274.
[38] Wikipedia (2019). *Grain boundary strengthening*.
[39] Facchini, D. (2012). Biomedical nanocrystalline metals and alloys: structure, properties and applications. In *Nanomedicine*, Elsevier, 36–67.
[40] Nguyen, N.-V., Pham, T.-H., Kim, S.-E. (2019). Strain rate-dependent behaviors of mechanical properties of structural steel investigated using indentation and finite element analysis. *Mechanics of Materials*, 137: 103089.
[41] Hu, X., Houtte, P. V., Liebeherr, M., Walentek, A., Seefeldt, M., Vandekinderen, H. (2006). Modeling work hardening of pearlitic steels by phenomenological and Taylor-type micromechanical models. *Acta Materialia*, 54(4):1029–1040.
[42] Russo, R., Mata, F. A. G., Forest, S., Jacquin, D. (2020). A Review on Strain Gradient Plasticity Approaches in Simulation of Manufacturing Processes. *Journal of Manufacturing and Materials Processing*, 4(3):87.
[43] Taylor, G. (1938). Plastic strain in metals, Twenty-Eighth May Lect. to Inst. *Met*, 62:307–325.
[44] Nix, W. D., Gao, H. (1998). Indentation size effects in crystalline materials: A law for strain gradient plasticity. *Journal of the Mechanics and Physics of Solids*, 46(3):411–425.
[45] Stölken, J., Evans, A. (1998). A microbend test method for measuring the plasticity length scale. *Acta Materialia*, 46(14):5109–5115.
[46] Nye, J. F. (1953). Some geometrical relations in dislocated crystals. *Acta Metallurgica*, 1(2):153–162.
[47] Ashby, M. F. (1970). The deformation of plastically non-homogeneous materials. *The Philosophical Magazine: A Journal of Theoretical Experimental and Applied Physics*, 21(170):399–424.
[48] Nguyen, N.-V., Pham, T.-H., Kim, S.-E. (2019). Strain rate sensitivity behavior of a structural steel during low-cycle fatigue investigated using indentation. *Materials Science and Engineering: A*, 744:490–499.